

Kinematic Closure of Drop Impact

Mete Abbot^{1,*} and Daniel Bonn^{1,†}

¹ *Van der Waals-Zeeman Institute, Institute of Physics,
University of Amsterdam, Science Park 904, 1098 XH Amsterdam, Netherlands*
(Dated: May 13, 2026)

Existing models for droplet impact prescribe the spreading contact time and effective spreading velocity from asymptotic arguments, which prevents a self-consistent prediction of the maximum spreading ratio across regimes. Here, the total spreading time and characteristic spreading velocity are derived directly from the energy balance, with explicit capillary and viscous contributions. Multiplying this time and velocity to obtain the maximum spreading diameter yields a closed, unified scaling law for the maximum spreading ratio of wetting drops across inertio-capillary and inertio-viscous regimes. The resulting expression quantitatively collapses the present measurements and literature data over wide ranges of Weber and Ohnesorge numbers, droplet sizes, and surface wettabilities without prefactors that need to be adjusted to a certain regime.

The impact of drops on solid surfaces is a key step in processes across vastly different scales: from the environmental transport of rainfall and the deposition of respiratory aerosols, to the precision of ink-jet printing and pesticide distribution [1, 2]. Despite over a century of study [3], establishing a universal prediction for the maximum spreading diameter D_{\max} of a droplet of initial diameter D_0 impacting on a solid surface remains an open problem due to the vast possible parameter space (Fig. 1). Energy conservation provides robust descriptions of the asymptotic inertio-capillary and inertio-viscous limits, leading to the well-known scalings $\beta_{\max} \equiv D_{\max}/D_0 \sim \text{We}^{1/2}$ and $\beta_{\max} \sim \text{Re}^{1/5}$ in their respective regimes, where We is the Weber number and Re the Reynolds number [4–7]. Building on these limits, several authors have proposed “bridging” frameworks that allow to collapse data, most prominently the Padé-type interpolation in terms of the impact parameter $P = \text{We} \text{Re}^{-2/5}$ introduced by Laan *et al.* [8] and subsequently refined or reinterpreted in various contexts [9, 10].

However, it has become increasingly clear that such empirical P -bridging is not universally valid across the full (We, Oh) space. For large Ohnesorge numbers, direct numerical simulations and theory show that viscous dissipation rapidly fills the drop volume, leading to a qualitatively new inertio-viscous regime [12–14] that is not fully captured by classical theories which calculate the main dissipation near the moving contact line [7, 8]. At the other extreme of low impact energy (small P), even for low-viscosity liquids, experiments reveal that the “capillary” branch of the Padé fit does not represent a purely inertial-capillary balance: a fraction of the kinetic energy is dissipated during the short impact phase, modifying both the effective prefactor and the apparent scaling exponent relative to the ideal $\text{We}^{1/2}$

law [8, 9, 11]. These discrepancies are clearly visible when $\beta_{\max} \text{Re}^{-1/5}$ is plotted against P for comprehensive datasets [8, 11–13, 15], as shown in Fig. 2a.

An additional subtlety at low velocities is the finite-volume, finite-wetting “baseline” spreading present even at zero impact velocity. Lee *et al.* [9] showed that dynamic wetting and contact-line pin-

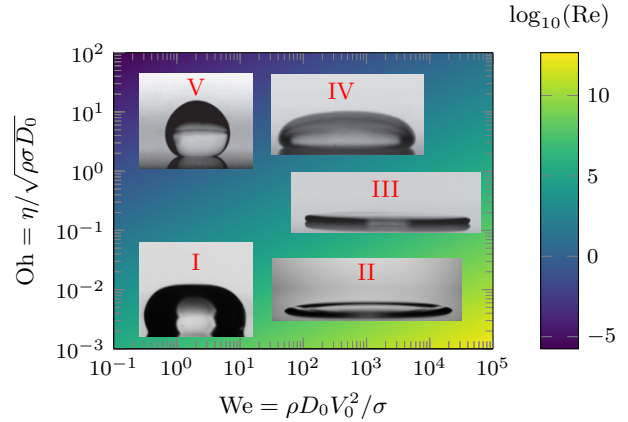


FIG. 1: Droplet morphology at maximum spreading across the parameter space.

Vertical axis is the Ohnesorge number $\text{Oh} = \eta/\sqrt{\rho\sigma D_0}$; horizontal axis is the Weber number $\text{We} = \rho D_0 V_0^2/\sigma$, where η is the dynamic viscosity, ρ density, σ surface tension, D_0 initial droplet diameter, and V_0 fluid velocity before impact. Background color mapping represents Re numbers. Insets correspond to scaling limits: in regime I (low We , low Oh), D_{\max} scales as $\text{We}^{1/2}$ [8–10]; in regimes II, III, and IV (high We), as $\text{Re}^{1/5}$ [5, 6, 11, 12]; and in regime V (low We , high Oh), as $\text{Re}^{1/3}$ [12].

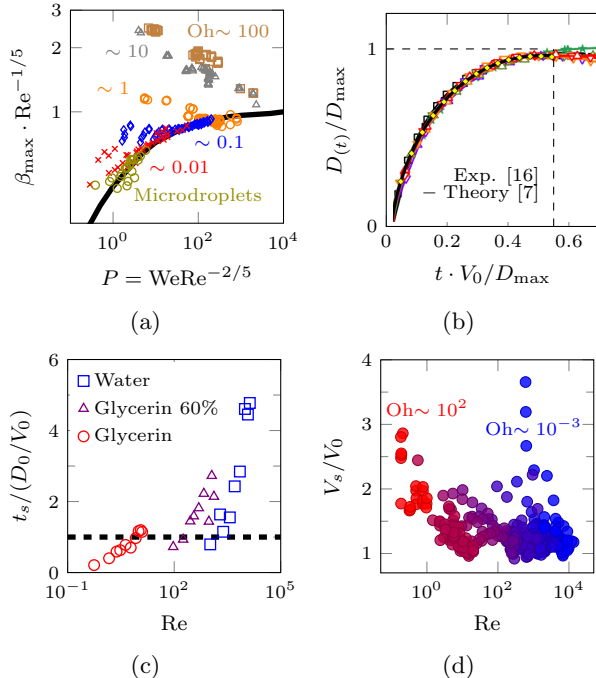


FIG. 2: **Predictive conundrum.** (a) Maximum spreading ratio β_{\max} based on the optical width, multiplied by $\text{Re}^{-1/5}$ for better visibility, versus impact parameter $P = \text{We} \text{Re}^{-2/5}$ from the experiments of [12, 13, 17] at Ohnesorge numbers between 0.01 and 100. The solid black line represents the empirical fit between the “classical regimes” using a Padé approximant proposed in [8]. (b) The kinematic universality of drop spreading of various liquids on various surfaces suggests a unified physical scaling exists [16]. (c) The experimental spreading time t_s from [13, 15] does not correlate with the inertial timescale. (d) The characteristic velocity V_s across the Ohnesorge scale deviates from V_0 (combined data from this work and [13, 15]) in a way that is independent of Re .

ning induce a nontrivial zero-velocity spreading ratio β_0 . By normalizing the measured spreading by β_0 to account for this capillary energy state, the apparent low- P scatter is removed, rendering the excess inertia-driven spreading more amenable to a unified description. Nonetheless, even in the idealized case, recent simulations show that the Laan-type interpolation still does not coincide with the true hydrodynamic solution at small P and large Oh [13, 14]. This indicates that the residual discrepancies are rooted not only in wetting and finite-volume geometry, but also in how viscous dissipation during impact and spreading is modeled.

In parallel with these developments, recent work has revealed a simple kinematic universality for droplet spreading. Gorin *et al.* [16] showed that the temporal evolution of the spreading diameter collapses onto a single curve when rescaled *post-facto* by D_{\max} and the impact velocity V_0 (Fig. 2b). Motivated by this observation, we posit that the maximum spreading ratio β_{\max} is governed by the kinematic relation

$$\beta_{\max} \equiv \frac{D_{\max}}{D_0} = \frac{V_s t_s}{D_0}, \quad (1)$$

where V_s is an effective average spreading velocity. Whereas the original kinematic framework implicitly assumed $V_s \sim V_0$ [16], we explicitly distinguish V_s from the impact velocity V_0 to account for systematic deviations from inertial scaling ($V_s = V_0$), which become pronounced in the low- P and high- Oh regimes [11–15].

Eq. (1) is purely kinematic and valid regardless of the experimental conditions or liquid properties. The predictive difficulty arises because V_s and t_s are *a priori* unknown dynamical outputs. Existing models predict spreading times representing asymptotic values of t_s for specific regimes: inertial ($\tau_i \sim D_0/V_0$) [4, 6, 11, 16], inertio-capillary ($\tau_{ic} \sim \sqrt{\rho D_0^3/\sigma}$) [13, 14], or viscous ($\tau_v \sim \rho D_0^2/\eta$) [12]. However, as shown in Fig. 2c and discussed in detail below, measured spreading times do not follow any single asymptotic timescale across the parameter space; instead, they continuously interpolate between these limits. Likewise, Fig. 2d demonstrates that the characteristic spreading velocity V_s systematically departs from V_0 . Taking t_s and V_s from asymptotic limits inherently constrains the resulting models to discrete regimes, complicating the description of the continuous physics of energy transfer across the parameter space.

In this Letter, we resolve these constraints by treating the spreading time t_s and the characteristic velocity V_s not as predefined inputs, but as emergent dynamical quantities determined self-consistently from the energy balance. We solve the energy balance directly for t_s and V_s , explicitly retaining both capillary storage and viscous dissipation. This yields a unified spreading timescale that continuously bridges the inertial, viscous, and capillary regimes, and an associated velocity scale that captures the observed deviations from $V_s = V_0$. Substituting these self-consistent kinematic scales into Eq. (1) leads to a unified scaling law for β_{\max} that remains valid across a wide physical landscape, from inviscid to highly viscous liquids and from low to high impact energies.

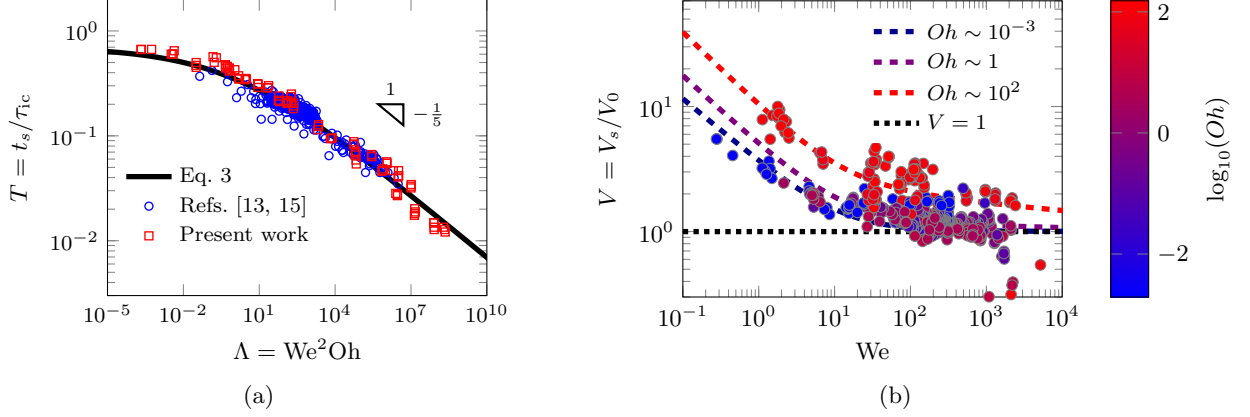


FIG. 3: **Kinematic closure.** (a) Dimensionless spreading time $T = t_s / \tau_{ic}$ as a function of the damping parameter $\Lambda = We^2 Oh$. Data are from this work and [13, 15], solid line is Eq. 3. (b) Characteristic spreading velocity $V = V_s / V_0$ as a function of We . Data are from [12, 13, 15].

We validate our predictions against $\sim 1,000$ experiments, combining this work’s measurements with a comprehensive literature dataset. The new experiments are used to expand the range of existing data beyond the optical or time resolution limits of literature experiments, using a Phantom v7510 high-speed camera (temporal resolution $\sim 10 \mu s$, spatial resolution $\sim 10 \mu m / px$). The liquids used are water, glycerol, and silicone oil 10 Pa·s. The combined dataset spans five orders of magnitude in viscosity (10^{-3} –45 Pa·s), droplet sizes from $30 \mu m$ to 4 mm, and contact angles from 0° to 140° [6, 8, 9, 12, 13, 17–25]. For the cases with contact angle $\theta = 180^\circ$ (no real contact), we compare our predictions with 1,348 numerical simulations of ideal non-wetting surfaces [14], and 126 experiments with balloons filled with viscous liquids [26].

To determine the characteristic spreading time t_s , we solve the energy balance ($E_k + E_{s,0} \approx E_{s,f} + W_\nu$). We explicitly retain the surface energy contribution ($E_{s,f} \sim \sigma D_{\max}^2$) to ensure a smooth transition to the thermodynamic wetting limit (see Supplementary Material S2). The viscous work W_ν is initially integrated throughout the spreading phase, capturing the geometric crossover from boundary-layer dissipation to volume-limited lubrication flow. Since both regimes have the same viscosity dependence ($\eta^{-1/5}$), they are combined into a single effective dissipation term in the form of volume-limited lubrication flow. (see Supplementary Material S3 and S4 for the detailed derivation).

The resulting energy balance is:

$$\mathcal{E} \approx V^2 T^2 + \Lambda V^6 T^5, \quad (2)$$

where $\mathcal{E} = 1 + 12/We$ is the total dimensionless en-

ergy density, $T = t_s / \tau_{ic}$ is the dimensionless time, $V = V_s / V_0$ is the normalized velocity, and the unified damping parameter $\Lambda = We^2 Oh$ emerges naturally from nondimensionalization.

Although Eq. (2) implicitly defines the spreading time, its physical behavior is best understood through its asymptotic limits. In the inviscid limit ($\Lambda \rightarrow 0$), the viscous term vanishes, yielding $T_{in} \approx \sqrt{\mathcal{E}} / V$. In contrast, in the highly viscous limit ($\Lambda \gg 1$), dissipation dominates, resulting in a scaling of $T_{visc} \approx (\Lambda V^6 \mathcal{E}^{-1})^{-1/5}$. To capture the continuous transition, we construct a matched asymptotic interpolation using the harmonic mean ($T^{-1} \approx T_{in}^{-1} + T_{visc}^{-1}$) that recovers the correct limits while maintaining monotonicity:

$$\begin{aligned} T &\approx \frac{\sqrt{\mathcal{E}}}{V} \left[1 + (\Lambda V \mathcal{E}^{3/2})^{1/5} \right]^{-1} \\ &\approx T_0 \left[1 + \Lambda^{1/5} \right]^{-1}. \end{aligned} \quad (3)$$

The second equality simplifies the expression for high-impact energies ($\mathcal{E} \rightarrow 1$ and $V \rightarrow 1$). In the inertio-capillary limit, the spreading time is governed by the prefactor T_0 , which is obtained by balancing the capillary restoring force $F \sim \sigma D_{\max} \sim \sigma V_s T_s$ against the droplet inertia $ma \sim (\frac{\pi}{6} \rho D_0^3) (V_s / t_s)$, which yields $t_s = \sqrt{(\pi/6) \rho D_0^3 / \sigma} = T_0 \tau_{ic}$, where the geometric coefficient $T_0 = \sqrt{\pi/6}$. Fig. 3a demonstrates that this approximation achieves a collapse of a wide range of experimental data.

To close the kinematic description (Eq. (1)), we must couple this unified timescale with the physically relevant length and velocity scales.

For the length scale, we distinguish the *contact*

diameter D_c from the *optical* width D_w . Because D_w remains finite even as true contact vanishes ($D_c \rightarrow 0$) at low We , utilizing D_c provides a more strict bound on the active viscous dissipation area. This distinction is strictly necessary to determine V_s and unify literature data. We derive an approximate geometric relationship, $\beta_w \approx \frac{1}{4}\beta_c^2 + 1$ for $\beta_c \leq 2$ (see Supplemental Material S1), ensuring the length scale reflects the physically active dissipation area.

Regarding the characteristic spreading velocity V_s , both established and recent models assume kinematic linearity ($V_s \sim V_0$) [4, 13]. More sophisticated low-viscosity-based models ($Oh \sim 10^{-3}$) incorporate hydrodynamic braking due to viscous dissipation within a spreading lamella feeding mass into a toroidal rim [6, 7, 11]. For liquids with a higher viscosity ($10^{-3} \leq Oh \leq 1$), more accurate empirical power-law fits of the form $We^a Re^b$ [15] have been proposed. Although effective in their respective regimes, these models do not provide a unified physical description of the velocity scaling that remains valid across the full range $10^{-3} \leq Oh \leq 10^3$.

However, the energy balance (Eq. (2)) imposes a constraint on the scaling of spreading velocity as:

$$V \approx \sqrt{\mathcal{E}} [T^6 + \Lambda \mathcal{E}^2 T^5]^{-1/6}. \quad (4)$$

Since contact time T is independently determined by Eq. (3), Eq. (4) becomes a self-consistent closure for the characteristic velocity without relying on empirical inputs. For practical applications, explicit, time-independent approximations can be used. For instance, $V = \sqrt{\mathcal{E}}$ is the zeroth-order limit for inviscid liquids ($Oh \ll 1$). The viscous damping contribution can be further approximated as $\sqrt{1 + Re^{-2/5}}$, a form inspired by boundary-layer theory.

This theoretically resolves the ‘‘Glycerol-Water Paradox’’ observed in experiments [11–13, 15] where highly viscous fluids spread faster than inviscid ones, for the same impact velocity V_0 . Furthermore, in the limit of low-energy deposition ($We \ll 1$), Eq. (4) correctly predicts that the characteristic spreading velocity can exceed the impact velocity by an order of magnitude ($V \gg 1$), as the spreading is enhanced by capillary forces. The agreement of this approximation with experiments from this work as well as from [12, 13, 15] is shown in Fig. 3b.

The kinematic closure is achieved by substituting the unified timescale (Eq. (3)) and the velocity closure (Eq. (4)) directly into the kinematic relation, Eq. (1). The resulting unified scaling law is:

$$\begin{aligned} \beta_{\max} &= VT\sqrt{We} \\ &\approx \sqrt{We\mathcal{E}} \left[1 + (\Lambda \mathcal{E}^2)^{1/5} \right]^{-1}. \end{aligned} \quad (5)$$

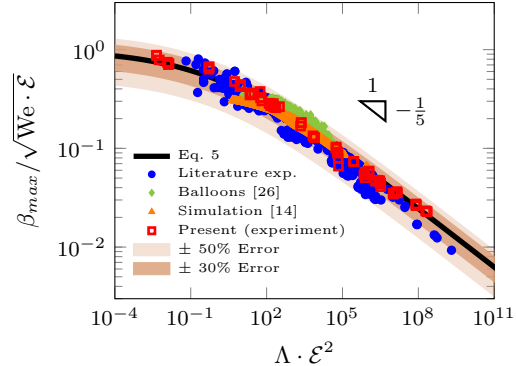


FIG. 4: Unified scaling of maximum spreading. Normalized spreading ratio $\beta_{\max}/\sqrt{We \cdot \mathcal{E}}$ plotted against the unified damping parameter $\Lambda \mathcal{E}^2$, following Eq. (5). The curve collapses $\sim 1,000$ experiments spanning extensive physical ranges (surface tension 0.02–0.5 N/m, viscosity 10^{-3} –45 Pa-s, diameter 30 μm –15 mm, impact velocity ≤ 40 m/s, and contact angle $\theta \in [0^\circ, 180^\circ]$), obtained in this work and sourced from the literature [6, 8, 9, 12–14, 17–26]. Because perfectly non-wetting cases ($\theta = 180^\circ$) lack a true contact area, they are restricted to cases where the drop width can be approximated as the contact diameter ($\beta_w \approx \beta_c$, i.e., $\beta > 2$). 30% and 50% error margins are shaded.

Since V within the viscous correction varies weakly across the explored parameter space, it is evaluated at leading order as $V \sim \sqrt{\mathcal{E}}$, reducing the damping term to $\sim \Lambda \mathcal{E}^2$. This controlled zeroth-order closure preserves the correct inertial and viscous asymptotic limits while providing a unified description across the full (We, Re) space without the need for adjustable or fitted parameters. In the inertial limit ($\Lambda \rightarrow 0, We \gg 1$), the denominator of Eq. (5) approaches unity, recovering the classical $\beta_{\max} \sim We^{1/2}$ scaling. Conversely, in the viscous limit ($\Lambda \gg 1$), the damping term dominates to yield $\beta_{\max} \sim \Lambda^{-1/5} We^{1/2} \sim Re^{1/5}$, a result consistent with both boundary-layer and lubrication theory.

A quantitative assessment of the proposed unified closure yields a mean error of just 10.15% for all wetting impacts ($\theta < 180^\circ$), demonstrating high predictive accuracy across physical regimes and length scales.

Minor geometric refinements may be useful near asymptotic limits, such as subtractive β_0 corrections for finite wettability at low We [9, 10, 27], or accounting for the toroidal rim as a momentum sink at high inertia, which slightly reduces the effective

velocity and spreading ratio [6, 7]. Another low We limit is the deposition limit for highly viscous liquids ($Oh > 100$), where the north pole of the drop does not deform and the boundary layer is limited near the contact area, leading to the scaling of $\beta \sim Re^{1/3}$ as reported in [12]. While our unified framework does not formally extract this discrete asymptotic exponent, the resulting continuous kinematic curve effectively envelops this extreme viscous space. Consequently, the highly viscous data from [12] are fully captured within the proposed curve (Fig. 4) with negligible quantitative deviation from Eq. (5). Furthermore, minor gravitational effects have been discussed and quantified in [12, 13].

The unified closure assumes that the droplet wets the substrate and has a well-defined contact area. Consequently, it does not consider perfectly non-wetting or levitating impacts, such as balloons [26], the Leidenfrost effect [28], the inverse Leidenfrost effect [29], or idealized non-wetting numerical simulations $\theta = 180^\circ$ [14]. By restricting our scope to actual fluid-solid contact ($\theta < 180^\circ$), the spreading is amenable to a single, unified kinematic description. Nevertheless, we empirically demonstrate that for highly deformed impacts ($\beta_w \geq 2$), the optical width closely approximates the physical contact diameter ($D_w \approx D_c$), allowing even these idealized non-wetting cases to align with the proposed scaling (as shown in Fig. 4).

In summary, classical drop-impact models prescribe spreading time and velocity from asymptotic limits, leading to deviations across transitional regimes. By solving the energy balance directly for these kinematic scales, we obtain a unified description governed by the single damping parameter $\Lambda = We^2 Oh$. The resulting scaling law for maximum spreading, free of asymptotic constraints and adjustable prefactors, collapses data over wide parameter ranges and resolves deviations from prior interpolations. This framework demonstrates that drop impact is a continuous process, amenable to a single predictive theory.

Acknowledgments — We gratefully acknowledge Peichun Amy Tsai, Detlef Lohse, Vatsal Sanjay, Loren Jørgensen, Lihui Liu, and Etienne Jambon-Puillet for both valuable discussions and providing experimental data. We also thank Martin Wörner and Zhifeng Hu for sharing their datasets. We thank Paul Kolpakov, Twan Spuijbroek, Eise Zimmerman, Jort Cornelissen, and Tessa Koekoek, for their help with the experimental setup and data collection.

* m.abbot@uva.nl

† d.bonn@uva.nl

- [1] C. Josserand and S. T. Thoroddsen, Annual review of fluid mechanics **48**, 365 (2016).
- [2] A. L. Yarin, Annu. Rev. Fluid Mech. **38**, 159 (2006).
- [3] A. M. Worthington, *The splash of a drop* (Society for Promoting Christian Knowledge, 1895).
- [4] C. Clanet, C. Béguin, D. Richard, and D. Quéré, Journal of Fluid Mechanics **517**, 199 (2004).
- [5] J. Eggers, M. A. Fontelos, C. Josserand, and S. Zaleski, Physics of fluids **22** (2010).
- [6] I. V. Roisman, Physics of Fluids **21** (2009).
- [7] J. M. Gordillo, G. Riboux, and E. S. Quintero, Journal of Fluid Mechanics **866**, 298 (2019).
- [8] N. Laan, K. G. De Bruin, D. Bartolo, C. Josserand, and D. Bonn, Physical Review Applied **2**, 044018 (2014).
- [9] J. B. Lee, N. Laan, K. G. de Bruin, G. Skantzaris, N. Shahidzadeh, D. Derome, J. Carmeliet, and D. Bonn, Journal of Fluid Mechanics **786**, R4 (2016).
- [10] T. C. de Goede, K. G. de Bruin, N. Shahidzadeh, and D. Bonn, Physical review fluids **4**, 053602 (2019).
- [11] M. Abbot, M. Lannert, A. Kiran, S. Bakshi, J. Hussong, and I. V. Roisman, Journal of Fluid Mechanics **996**, A10 (2024).
- [12] L. Jørgensen, Physical Review Fluids **9**, 083601 (2024).
- [13] L. Liu, G. Cai, W. Wang, B. He, and P. A. Tsai, Journal of Fluid Mechanics **1018**, A42 (2025).
- [14] V. Sanjay and D. Lohse, Physical review letters **134**, 104003 (2025).
- [15] Y. T. Aksoy, P. Eneren, E. Koos, and M. R. Vetrano, Physics of Fluids **34** (2022).
- [16] B. Gorin, G. Di Mauro, D. Bonn, and H. Kellay, Langmuir **38**, 2608 (2022).
- [17] J. McLauchlan, J. S. Walker, V. Sanjay, M. Jalaal, J. P. Reid, A. M. Squires, and A. Souslov, Proceedings of the National Academy of Sciences **122**, e2507309122 (2025).
- [18] J. Du, X. Wang, Y. Li, Q. Min, and X. Wu, Langmuir **37**, 7582 (2021).
- [19] L. Liu, B. He, W. Wang, G. Cai, and P. A. Tsai, Physical Review Fluids **8**, 073602 (2023).
- [20] L. Cheng, Industrial & Engineering Chemistry Process Design and Development **16**, 192 (1977).
- [21] M. Pasandideh-Fard, Y. Qiao, S. Chandra, and J. Mostaghimi, Physics of fluids **8**, 650 (1996).
- [22] H. Marmanis and S. Thoroddsen, Physics of fluids **8**, 1344 (1996).
- [23] T. Naoe, M. Futakawa, R. G. Kenny, and M. Otsuki, Journal of Fluid Science and Technology **9**, JFST0002 (2014).
- [24] M. H. Iqbal, M. A. Quetzeri-Santiago, A. A. Castrejón-Pita, and J. R. Castrejón-Pita, Journal of Colloid and Interface Science , 139385 (2025).
- [25] M. Abbot, M. H. Iqbal, L. Liu, E. Koos, I. V. Roisman, J. Hussong, A. A. Castrejón-Pita, and J. R.

- Castrejón-Pita, *Journal of Colloid and Interface Science* **693**, 137570 (2025).
- [26] E. Jambon-Puillet, T. J. Jones, and P.-T. Brun, *Nature Physics* **16**, 585 (2020).
- [27] M. Wörner, *International Journal of Multiphase Flow* **167**, 104528 (2023).
- [28] I. Roisman, J. Breitenbach, and C. Tropea, *Journal of Fluid Mechanics* **842**, 87 (2018).
- [29] K. Isukwem, C.-A. Charles, T. Phou, L. Ramos, C. Ligoure, E. Hachem, and A. Pereira, *Journal of Fluid Mechanics* **1002**, A32 (2025).